Inorganic Chemistry

Article

pubs.acs.org/IC

Understanding the Relationships between Structural Features and Optical/Magnetic Properties When Designing $Fe_{1-x}Mg_xMoO_4$ as Piezochromic Compounds

Veronica Blanco-Gutierrez, Alain Demourgues, Olivier Toulemonde, Alain Wattiaux, Olivier Nguyen, and Manuel Gaudon*

Université de Bordeaux, CNRS, ICMCB, 87 Avenue du Dr. Albert Schweitzer, 33608 F-Pessac Cedex, France

ABSTRACT: $Fe_{1-x}Mg_xMoO_4$ compounds with x = 0, 0.25, 0.5, 0.75, and 1.0 were obtained after annealing under inert gas at T = 700 °C. All of the compounds exhibit a pressure-induced and/or temperature-induced phase transition between the two polymorphs adopted by $AMoO_4$ compounds (A = Mn, Fe, Co, and Ni). For the $FeMoO_4$ compound, for both the α and the β allotropic forms, the structural features have been correlated to the magnetic properties, the Mössbauer signals, and the optical absorption properties to gain a better understanding of the phenomena at the origin of the piezo(thermo)chromic behavior. The different contributions of the Mössbauer signals were attributed to the different Fe^{2+} ions or Fe^{3+} ions from the structural data (Wyckoff positions, bond distances and angles) and were quantified. Furthermore, the low Fe^{3+} concentration (9 and 4 mol %, respectively, in the α and the β allotropic forms) was also quantified based on the magnetic susceptibility measurements. The net increase in the Fe^{3+} quantity in the α-form in comparison to the β-form, which is associated with the occurrence of Fe−Mo charge transfer, is at the origin of the important divergence of coloration of the two forms. To design new piezo(thermo)chromic oxides and to control the pressure (temperature) of this first-order phase transition, $FeMoO_4$−$MgMoO_4$ solid solutions were synthesized. The optical contrast between the two allotropic forms was increased due to magnesium incorporation, and the phase transition ($\beta \rightarrow \alpha$) pressure increased steadily with the Mg content. A new generation of nontoxic and chemically stable piezochromic compounds that are sensible to various pressures was proposed.

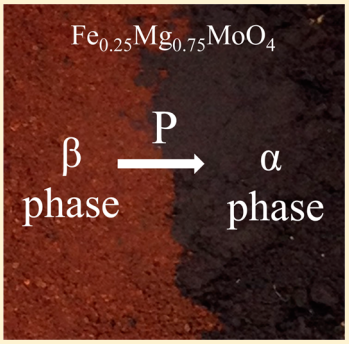

1. INTRODUCTION

Piezochromic behavior is one of the most interesting physical phenomena studied in materials science;[1−3] it can be exploited in the technological fields of smart paintings or sensor devices.[1] Materials with this property present a change of color after a mechanical stimulus, and, most of the time, the initial phase can be recovered after heating. Therefore, piezochromic and thermochromic behavior are linked phenomena in a reversible process.[1,4,5] Piezochromic materials can be of a different nature, such as inorganic complexes,[6,7] polymers,[8] or inorganic crystals,[1,2] and generally offer better chemical and physical stability. In this last case, the change of color is related to a first-order phase transition between two different crystal structures characterized by a transition pressure (P_{tr}).[9,10] Molybdate compounds are some of the most versatile inorganic materials with different technological applications such as catalysts or electronic devices,[11−13] but some molybdate compounds also present exploitable optical properties associated with piezochromic behavior. This is the case for $AMoO_4$ (where A = Co, Ni, Cu, Fe),[1,2,9,14] compounds, which present low transition pressure in comparison with other inorganic crystals, such as CdS,[15] which makes them useful as smart materials for daily life. In addition, recent studies have indicated the possibility of tuning up this transition pressure by means of chemical doping[9] or modifying the particle size,[2,9] which stabilizes the low or high coordination form. However, the presence of toxic A-elements (Co, Ni, Cu) in the general $AMoO_4$ formula leads us to focus our attention on the $FeMoO_4$ composition. This compound is a redox subproduct after the oxidation of alcohols and hydrocarbons when employing the $Fe_2(MoO_4)_3$ catalyst.[11,12,16] There are no reported studies concerning its piezochromic behavior. $FeMoO_4$ can be found in several allotropic forms[17] corresponding to the α and β phases and correlated through piezochromic and thermochromic phenomena at a 673 K transition temperature, at which the $\alpha \rightarrow \beta$ transformation occurs. Both the α and β phases crystallize with the $C2/m$ space group (S.G.) and are isomorphs with the homologous phases corresponding to $CoMoO_4$. Fe^{2+} cations are located in the distorted octahedral sites for both phases, and Mo^{6+} cations change from tetrahedral to octahedral coordination with the $\beta \rightarrow \alpha$ transition. When pressure is applied, four isolated $[MoO_4]$ tetrahedra in the β-phase are linked by edge-sharing to give a $[Mo_4O_{16}]$ tetramer of octahedral sites in the α-phase, which implies a 6.8% increment of the crystal density (from 4.37 g/cm^3 to 4.67 g/cm^3).[18] The crystal networks of both phases are illustrated in Figure 1.

Different synthesis routes can be employed to obtain these inorganic materials. In the past decade, the soft chemistry route has been considered to be a useful tool to obtain compounds

Received: October 27, 2014
Published: February 9, 2015

ACS Publications © 2015 American Chemical Society

DOI: 10.1021/ic5025845
Inorg. Chem. 2015, 54, 2176−2184

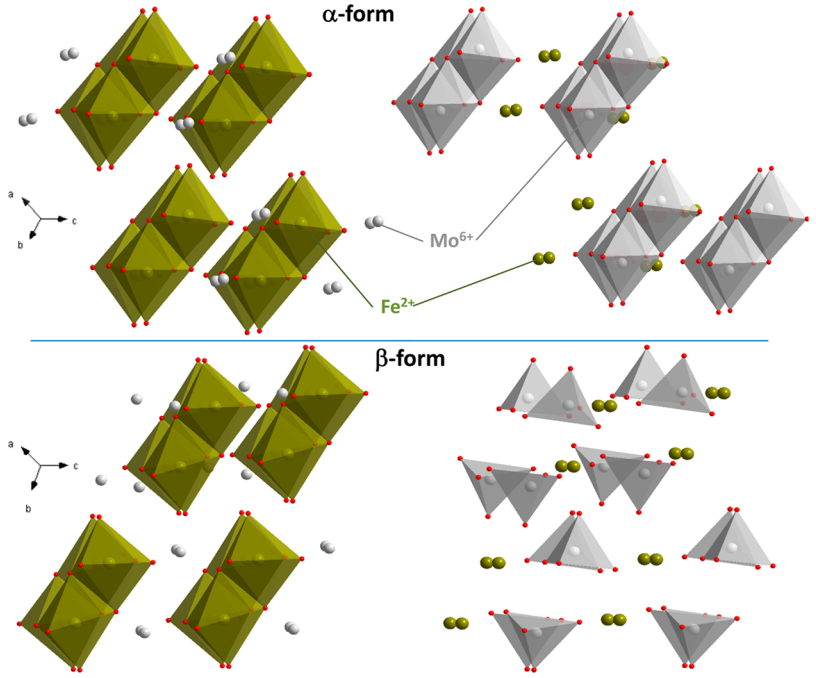

Figure 1. α-$FeMoO_4$ and β-$FeMoO_4$ representations highlighting the iron or the molybdenum polyhedron subnetwork.

with desirable particle sizes and morphology.[19,20] However, for the preparation of $AMoO_4$ materials, the synthesis route must be completed with a high-temperature step to dehydrate the $AMoO_4{\cdot}nH_2O$ phases that are obtained through soft-chemistry methods.[21,22] In this work, the solid-state route was used to obtain the desired crystallographic phase, leading to larger particles that generally offered better optical properties, because of a low scattering phenomenon.[23] We thus describe, for the first time, the piezochromic behavior of $FeMoO_4$. The structural, optical, and magnetic characterization of the $FeMoO_4$ compound and the influence of Mg^{2+} substitution for Fe^{2+} into $FeMoO_4$ on the piezochromic behavior have been studied.

2. EXPERIMENTAL SECTION

2.1. Synthesis Processes. Samples of $Fe_{1-x}Mg_xMoO_4$ with x = 0, 0.25, 0.5, 0.75, and 1—referenced as F, M25, M50, M75, and M, respectively—were prepared by the solid-state route employing stoichiometric amounts of $FeCl_2{\cdot}4H_2O$, $MgCl_2{\cdot}6H_2O$, and $(NH_4)_2MoO_4$ reactants. After homogenization of the reactants mixture by grinding in an agate mortar, the powder was placed in an alumina crucible and was thermally treated under an air atmosphere and then an argon atmosphere in two steps. First, the mixture was treated at 400 °C for 10 h under an air atmosphere with a heating rate of 1 °C/min, and then, after rehomogenization of the mixture by grinding, a second step under argon was performed at 700 °C for 10 h with the same heating rate. The powder was left to cool inside the furnace to 200 °C for each step. Sample M was prepared in the same manner as the others, but in air, and an additional final step at 1000 °C for 24 h was needed. For the final treatment, the powder was placed in a sealed platinum tube of argon atmosphere and the temperature was increased at a rate of 1 °C/min. For all samples, the final powder was obtained using slow cooling (2 °C/min); compounds exhibiting the pure β-phase were then obtained in all cases. All of the $(Fe,Mg)MoO_4$ samples were then subjected to progressive pressure values up to 17.5 kbar to induce the $\beta \rightarrow \alpha$ phase transition.

2.2. Characterization Techniques. The structural characterization of the samples was performed by X-ray diffraction employing a Philips Model PW 1820 apparatus equipped with a $K\alpha_1/K\alpha_2$ source and a copper anticathode. Diffraction patterns were collected with a 2θ step of 0.02° between 20° and 40° with a counting rate of 10 s per step in the routine mode. The structures were studied by full pattern matching of the corresponding diagrams.

Diffuse reflectance spectra $R(\lambda)$ were recorded at room temperature using a Cary 17 spectrophotometer with an integration sphere in the wavelength range of 350−850 nm and a 1 nm step and a 2 nm bandwidth. Halon was used as a white reference for the blank. Visible−near-infrared (vis-NIR) spectroscopic analyses were also conducted in diffuse reflectance mode with a Konica−Minolta Model CM-700d spectrophotometer equipped with an integrating sphere coated with polytetrafluoroethylene (PTFE). Measurements were performed for wavelengths varying from 200 nm up to 2500 nm, in the Specular Component Excluded (SCE) mode. A white calibration cap (Model CM-A177, ceramic) was used as a white reference, and the standard D65 (daylight, color temperature: 6504 K) with a 10° observer angle (CIE1964) was used as an illuminant. Only the ultraviolet−visible (UV-vis) wavelength range and the La^*b^* space parameters (where L is the luminosity; a^* the green-to-red axis coefficient; and b^*, the yellow-to-blue axis coefficients) were considered. No computing mathematics treatment was performed because the apparatus directly sets the La^*b^* chromatic parameters. The colorimetric parameter a^* is descriptive of the green−red hue axis. This parameter was chosen to quantify the α and β forms ratio inside the powder sample during the phase transition because the a^* value is very different for the two allotropic forms. A home-built instrument equipped with a photomultiplier allowed the collection of the reflected intensity in the 400−680 nm range from 40 °C to −260 °C (using a cooling rate of ∼5 K/min).

Magnetic susceptibility was measured using a Quantum Design XL-SQUID magnetometer in the temperature range of 2−300 K in the presence of 0.2 T magnetic fields. Once the magnetic field was applied at room temperature, magnetic moment data were collected while the sample was cooled to 2 K, defining a field-cooled cooling (FCC) mode. Then, the sample was heated to 300 K without stopping the data collection, defining a field-cooled warming (FCW) mode.

Mössbauer measurements were performed with a constant acceleration Halder-type spectrometer using a room-temperature ^{57}Co source (Rh matrix) in the transmission geometry. The polycrystalline absorbers containing ∼10 mg/cm^2 of iron were used to avoid the experimental widening of the peaks. The velocity was calibrated using pure iron metal as the standard material. To evaluate

DOI: 10.1021/ic5025845
Inorg. Chem. 2015, 54, 2176−2184

the Fe^{3+} and Fe^{2+} local environments of the studied ferrite compounds, ^{57}Fe Mössbauer spectra were collected at 293 K. The spectra were fitted considering the signal with peaks of the Lorentzian profile. The position, the intensity, and the width of each peak are refined. The hyperfine parameters for the various Fe sites were then deduced.

The pressure was applied in a uniaxial way, following the details described in a previous study.[9] The pressure was applied by a home-built scalepan balance in which a counter mass was used in a lever system with a pivot point to multiply the mechanical force (effort) that can be applied on the piston of the pellet matrix.[9] The powder samples were introduced in a pellet matrix with a varying diameter from 6 mm to 13 mm, depending on the desired pressure.

3. RESULTS

3.1. Structural, Optical, and Magnetic Characterization of $FeMoO_4$ Composition. The crystal structure of $FeMoO_4$ samples (F samples) was studied by full pattern matching refinement or Rietveld refinements using the $C2/m$ space group for both phases.[10] The extraction of the α and β-phase weight ratio after the highest pressure application (17.5 kbar) was performed using the X-ray diffraction (XRD) patterns. For the nonpressed and pressed F samples, the experimental and calculated XRD patterns, together with the differential signals for the as-prepared phases are represented in Figure 2, and the indexed diffraction peaks can be ascribed to the β and α phases (Figures 2a and 2b, respectively),[2] although some traces (~3 mol %) of the β-phase were found in the diagram corresponding to the pressed sample. The sharp diffraction peaks observed in both patterns suggest a large coherent domain for both phases in accordance with particles of the micrometric size.[9] The cell parameter values obtained after the refinements, together with the reliability factors, are collected in Table 1 for both the β and α phase of the F samples, and they are in good agreement with other previously reported values.[18]

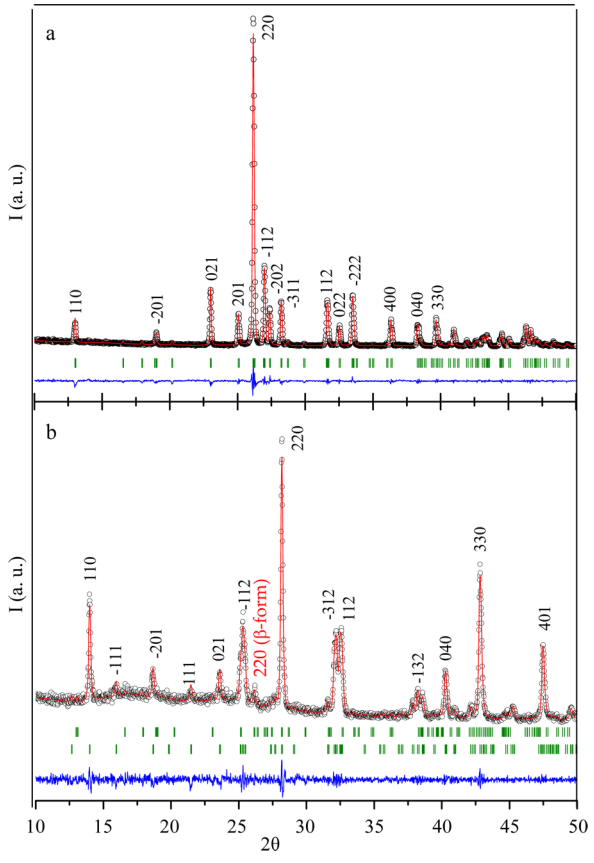

Figure 2. X-ray diffraction (XRD) patterns of (a) β-$FeMoO_4$ and (b) α-$FeMoO_4$. The calculated pattern obtained from the profile refinement of the experimental pattern, together with the difference between both, and the Bragg positions are also depicted.

The Kubelka–Munk transformation of the diffuse reflectance spectra versus the photon energy of the nonpressed and pressed F samples are presented in Figure 3. Both spectra can be described by a typical $^5T_2 \rightarrow {}^5E$ absorption band peaking at 1.0 eV, which can be assigned to Fe^{2+} in distorted octahedral sites. The lower K/S intensity of this band, in the case of the nonpressed sample (with pure β-form), may be related to not-as-distorted octahedral sites in this case and also with a lower refractivity index, because of a lower crystal density for the same composition.[2] At higher energy values, there is an absorption threshold that can be attributed to a charge transfer band (CTB) from O^{2-} (2p) to the Mo^{6+} (empty 4d), because the band position is sensitive to the change of the local environments of the Mo^{6+} ions.[10] A CTB displacement to the UV region is seen when going from the α phase to the β phase, because of a more covalent Mo–O bond related to the lower coordination sphere of the Mo^{6+} cation in the β-phase.[2] A schematization of the band diagram of the two allotropic forms is depicted in Figure 4. This shift in the $O^{2-} \rightarrow Mo^{6+}$ CTB is the origin of the different color between the nonpressed (brown) and the pressed (black) samples. The optical band gap energy (E_g) can be estimated by the classical Tauc approach[24] from the intercept of the tangents to the photon energy axis. Estimated values of ~1.1 and 1.7 eV have been found for the α and β phases, respectively, which is in agreement with the already reported value for the β-phase.[25] Already reported studies concerning the optical properties of the β and α phases of $CoMoO_4$ show a $O^{2-} \rightarrow Mo^{6+}$ CTB at 2.4 and 2.9 eV for the α and β phases, respectively.[10] The lower values found for the $FeMoO_4$ composition can be justified by taking into account the easy oxidation of Fe^{2+} into Fe^{3+}. Hence, the oxygen to molybdenum charge transfer is assisted by the Fe → O charge transfer. Such a metal(1)-to-oxygen-to-metal(2) charge transfer was previously shown for the $Co_{1-x}Mg_xMoO_4$ compound series[10] and with the (Mo,Cu) 1212 cuprate phase.[26] Moreover, Woodward et al.[27] have also discussed the occurrence of metal (A)-to-metal (W) charge transfer instead of oxygen-to-metal (W) charge transfer in AWO_4 wolframite phases when cation A can be easily oxidized. For the α phase, the charge transfer is located at an energy so low that the color of the α-$FeMoO_4$ compound is almost black, while a high infrared reflectivity is maintained; this behavior makes this compound very interesting as a cool-roof pigment.[28−31]

The piezochromic behavior at room temperature has been illustrated in Figure 5a. The phase transition from the low-pressure β-form (brown) to the high-pressure α-form (black) has been depicted after normalization of the α/β phase ratio associated with the a^* color parameter variation with pressure up to values of 17.5 kbar.[2] From this curve, a transition pressure (P_{tr}) value of 80 bar was estimated, which corresponds to 50% of the $\beta \rightarrow \alpha$ phase transition. This slightly higher value in comparison with that corresponding to $CoMoO_4$ microparticles (~35 bar)[2] is in accordance with the stabilization of the low-coordination phase, because of the slightly higher atomic radii and slightly lower electronegativity of the Fe^{2+} cation in comparison with Co^{2+}. A similar effect has been found when incorporating Mg^{2+} into the $CoMoO_4$ composition.[9]

DOI: 10.1021/ic5025845
Inorg. Chem. 2015, 54, 2176−2184

Table 1. Crystallographic Data Corresponding to the (Fe,Mg)MoO_4 Samples for Both the Low-Pressure (β) and the Low-Temperature (α) Phases and the Phase Content in the Powder Obtained after the Application of High Pressure

	phase content (mol %)	a (Å)	b (Å)	c (Å)	β (deg)	V (Å^3)	R_p	Rw_p
				Sample F				
α-form	3(1)	10.2949(2)	9.3953(2)	7.0731(1)	106.261(1)	656.77(2)	8.7	12.1
β-form	97(1)	9.807(1)	8.942(1)	7.6520(6)	114.065(7)	612.8(1)	6.9	9.0
				Sample M25				
β	27(1)	10.2943(4)	9.3873(5)	7.0621(3)	106.414(3)	654.64(5)	8.7	12.0
α	73(1)	9.784(2)	8.926(2)	7.649(1)	113.93(1)	610.6(2)	9.1	12.5
				Sample M50				
β	38(1)	10.2922(8)	9.3481(8)	7.0487(5)	106.617(4)	649.85(9)	11.9	16.1
α	62(1)	9.778(1)	8.910(1)	7.6372(8)	113.87(1)	608.5(1)	6.1	8.2
				Sample M75				
β	44(1)	10.2789(8)	9.318(1)	7.0300(5)	106.783(4)	644.7(1)	12.3	17.2
α	56(1)	9.723(2)	8.920(2)	7.630(1)	113.74(1)	605.8(2)	6.2	8.0
				Sample M				
β	100	10.2746(1)	9.2895(1)	7.02552(9)	106.8840(9)	641.65(2)	7.0	9.8

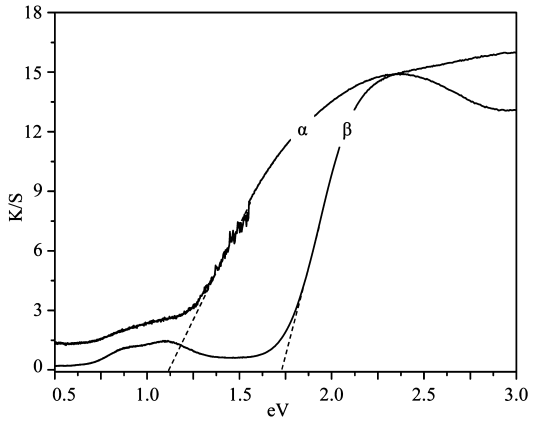

Figure 3. Kubelka–Munk transformation spectra (K/S) for the pressed and nonpressed F samples.

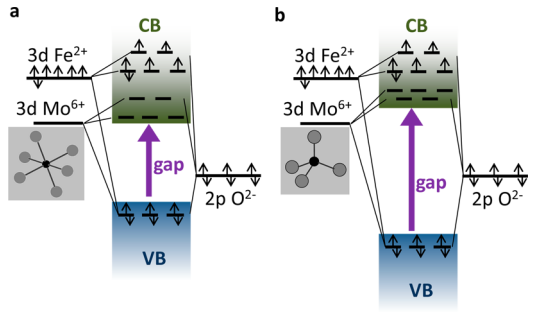

Figure 4. Schematization of the band diagram of the (a) α-$FeMoO_4$ and (b) β-$FeMoO_4$ allotropic forms. The conduction band (CB) and valence bands (VB) are roughly obtained by considering phonon dispersion of the constituting molecular orbitals.

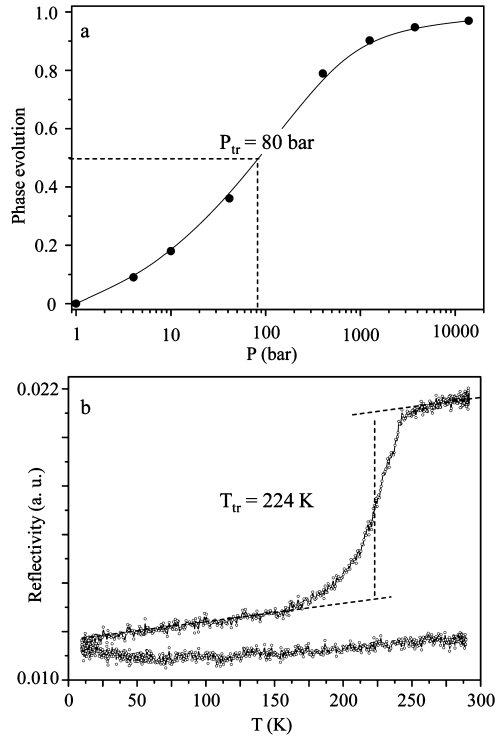

Figure 5. (a) Phase transformation with pressure from the $\beta \rightarrow \alpha$ form and (b) variation of the reflectivity spectra versus temperature for the $FeMoO_4$ composition.

The thermochromic behavior from the high-temperature β-form to the low-temperature α-form has been represented in Figure 5b. The transition causes a change in the optical properties of the $FeMoO_4$ compounds, which can be evaluated by means of reflectivity, allowing access to the integrated reflectivity in the 539-nm region that differs in K/S intensity between both phases. Upon cooling, the β–α transition allows determination of the transition temperature (T_{tr}) corresponding in a first approximation to ~50% mol of the β and α phases. As indicated in Figure 5b, T_{tr} was estimated at 224 K. The hysteresis curve is not complete, because the α-phase remains stable up to 673 K.[17]

The $\beta \rightarrow \alpha$ phase transition with temperature can be followed by means of magnetic measurements. Two aspects can be probed: (i) the occurrence of the structural phase transition highlighted by a thermal hysteresis between curves measured in the FCC and FCW modes, (ii) the occurrence of the proposed metal (A)-to-metal (W) charge transfer. The magnetic susceptibility measured under 2000 Oe in the 2–300 K temperature range is represented in Figure 6a. $FeMoO_4$ compound in the β phase (nonpressed sample) at 300 K was cooled to 2 K while measuring the susceptibility in the FCC curve. Afterward, the measurement was continued from 2 K to room temperature in the FCW susceptibility curve. The first noticeable change is related to the maximum of the magnetic

DOI: 10.1021/ic5025845
Inorg. Chem. 2015, 54, 2176–2184

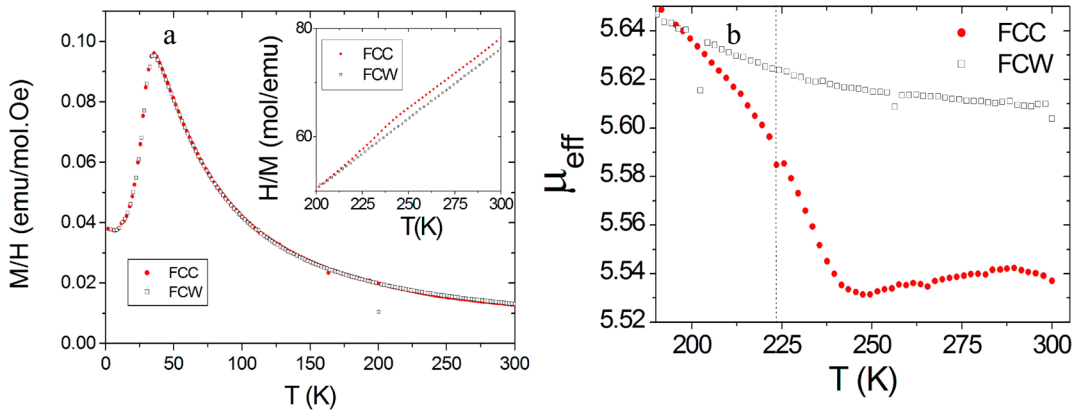

Figure 6. (a) Magnetic susceptibility measured at 2000 Oe in the temperature range of 2−300 K on the FCC mode (solid symbols) and FCW mode (open symbols) for the $FeMoO_4$ composition. The inset shows the inverse magnetic susceptibility around the $\beta \rightarrow \alpha$ phase transition. (b) Temperature dependence of the paramagnetic moment deduced from the magnetic susceptibility following a Curie−Weiss model; the parameter μ_{eff}^{FCC} corresponds to the paramagnetic moment shown by the β-phase, whereas the parameter μ_{eff}^{FCW} corresponds to the paramagnetic moment shown by the α-phase. Only a part of the thermal hysteresis is plotted.

susceptibility at T_N = 35 K, indicating a phase transition from the paramagnetic to antiferromagnetic state. Both the FCC and FCW curves match below T_N and show the same maximum at 35 K, suggesting a long-range magnetic order, which has been previously described.[18,31] The inset of Figure 6 is related to the $\beta \rightarrow \alpha$ phase transition. The inflection point shown on the FCC curve is in perfect accordance with the already estimated T_{tr} = 224 K from the diffuse reflectance curve. As expected, the curve measured on the FCW process does not show any features because the $\alpha \rightarrow \beta$ phase transition occurs at 673 K,[17] outside of the studied temperature range. Such measurements allow us to estimate the metal(1)-to-oxygen-to-metal(2) charge transfer from a Curie−Weiss analysis of the data. Figure 6b shows the temperature dependence of the paramagnetic moment extracted from a CW analysis of the magnetic susceptibility. It shows an increase from 5.53/5.54 μ_B for the β phase and up to 5.61 μ_B for the α phase. Considering the $Fe^{2+}Mo^{6+}O_4$ nominal valence distribution with a high-spin Fe^{2+} state and a nonquenched orbital moment hypothesis, a value of 5.47 μ_B for the paramagnetic moment should be found. The estimated paramagnetic moment for both phases is slightly higher than 5.47 μ_B, suggesting that the occurrence of a small Fe^{3+} state fraction should result in a small Mo^{5+} oxidation state fraction, to counterbalance the positive charge. This permanent presence of III and V oxidation states, respectively, for iron and molybdenum is caused by the metal-to-oxygen-to-metal charge transfer previously discussed. Considering the $Fe^{2+}_{1-x}Fe^{3+}_{x}Mo^{6+}_{1-x}Mo^{5+}_{x}O_4$ valence distribution and effective paramagnetic moments equal to 5.91 for high spin Fe^{3+} and 1.73 for spin-only Mo^{5+}, compositions with x = 0.09 or x = 0.20 would correspond to the α phase and the β phase, respectively. The charge transfer tendency is consequently also suggested by the magnetic susceptibility change, even if the paramagnetic magnetic moment of the Fe^{2+} is assumed to be fixed. That is why Mössbauer spectroscopy study, which is known as an iron chemical selective analysis, was conducted.

Figure 7 shows the Mössbauer spectra at room temperature corresponding to the Fβ and Fα samples (Figures 7a and 7b, respectively). The position, intensity (I) width (Γ) and quadripolar splitting of the Mössbauer signal contributions are reported in Table 2. The α-form and β-forms clearly present a different Mössbauer signal, despite their proximal structures. For the Fβ sample (Figure 7a), the spectrum can be described

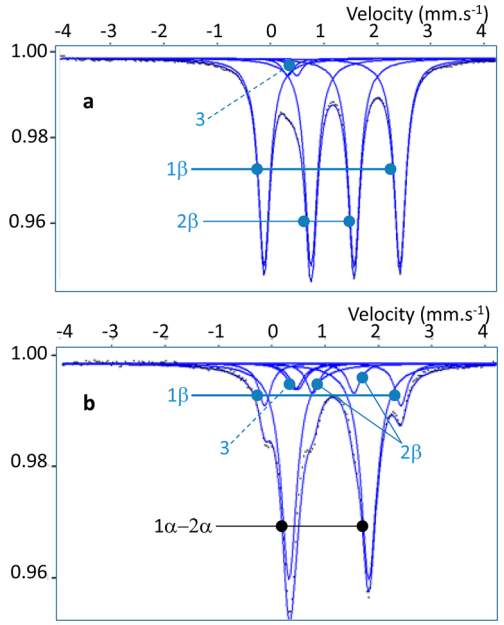

Figure 7. Mössbauer spectra (room temperature) on the (a) β form and (b) α form of $FeMoO_4$. All of the Fe^{2+} and Fe^{3+} contributions with notation corresponding to Table 2 are reported.

Table 2. F Samples (Pressed and Nonpressed Samples) Refined Parameters from Their Mössbauer Spectra

F sample	site number	δ (mm s^{-1})	Γ (mm s^{-1})	Δ (mm s^{-1})	content (mol %)
nonpressed (β)	1β	1.129	0.264	2.56	48
	2β	1.151	0.267	0.82	48
	3	0.432	0.255	0.17	4
pressed (β+α)	1α and 2α	1.057	0.349	1.51	72
	1β	1.127	0.283	2.57	11
	2β	1.140	0.284	0.78	8
	3	0.446	0.358	0.05	9

by two main doublets indexed to Fe^{2+} in site 1 (4i Wyckoff position) and site 2 (Wyckoff position 4h). The non-Lorentzian

DOI: 10.1021/ic5025845
Inorg. Chem. 2015, 54, 2176−2184

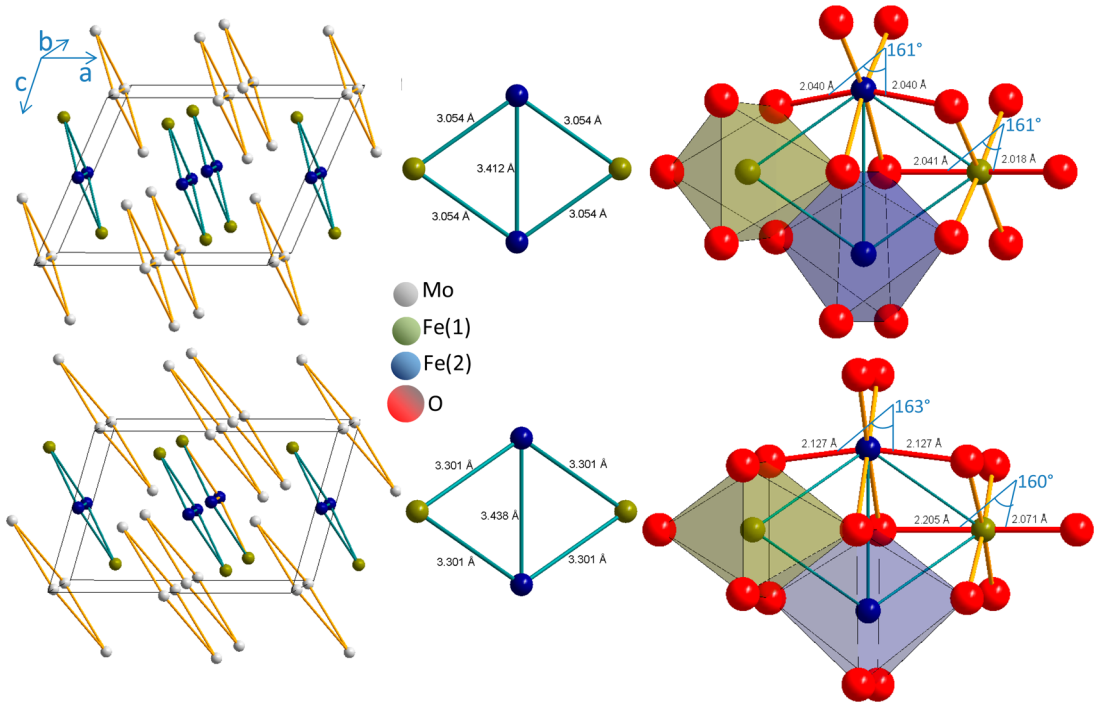

Figure 8. Structural representation of the α form (top row) and β form (bottom row). Also shown are a description of the cell with emphasis of the Mo and Fe tetramer disposition (left); the focus on a Fe tetramer along an axis projection (middle column); and a comparison of the Fe(1) and Fe(2) octahedral site distortions (right).

shape of the lines indicates the presence of an additional minor doublet (named site 3 in Table 2) attributed without any ambiguity to Fe^{3+} traces. From the chemical displacement (δ) and the quadripolar splitting (Δ) values, it has been determined to contain ~4% of Fe^{3+}. For the Fα sample (Figure 7b), the two doublets relative to the β sample were still detected, because ~19% of the compound remains in the high-temperature form. A complete transition induced by mechanical grinding from the β form to the α form is difficult to reach. In addition to this residual β-form doublet, the remainder of the spectrum can be fitted considering one main doublet attributed to Fe^{2+} and an additional minor doublet associated with the occurrence of 9% Fe^{3+}. The structural networks can be described for both phases as alternating iron-tetramer planes and molybdenum-tetramer planes, as can be observed in Figure 8. In both phases, there are two Wyckoff positions for the Fe^{2+} ions, site 1 and site 2, and in both phases, two Fe^{2+} ions in site 1 and two in site 2 are linked to form a tetramer. However, although the degree of distortion is very different for each Fe site in the case of the high-temperature form (β), in the case of the α phase, it is quite similar. Quantification of the degree of distortion for an octahedral site is a somewhat subjective calculation. Nevertheless, a clear way to compare the degree of distortion of the two iron Wyckoff positions in the two allotropic forms was found. The four compared octahedral sites (i.e., sites 1 and sites 2 in the α and β forms) have one of their three oxygen−metal−oxygen axes significantly more distorted than the two others: the O−Fe−O angles for the more distorted axes are ~160°, whereas the others are all >170°. Then, the global distortion of the octahedral sites can be qualified by taking into account the distortion of the most distorted axes. For the β-form, site 1 is significantly more distorted than site 2. In site 1, the Fe^{2+} cation is out of the center of the O−Fe−O axis, and in site 2, the two Fe−O bonds of the distorted axis have the same length and the angle O−Fe−O is less distorted (163°). For the α form, both site 1 and site 2 exhibit the same distortion angles (161°), and all of the Fe−O bonds have similar lengths. Thus, the four compared octahedral sites follow this growing order of distortion: site 1β < site 1α and site 2α < site 2β. The various quadripolar splittings reported in Table 2, which are linked to the degree of distortion of the interstitial sites, are in agreement with the previous classification. Another important observation is the increase of the Fe^{3+} rate from the high-temperature form to the low-temperature forms. This observation is in agreement with the slightly lower magnetic susceptibility of the α-phases, as previously discussed. Furthermore, the observation corroborates the possibility for a metal-to-oxygen-to-metal charge transfer from Fe to Mo. Thus, such charge transfer would be responsible for the occurrence of Fe^{3+} traces, because Mo in octahedral sites (in α form) is more ionic than in tetrahedral sites (in β form) and is therefore easier to reduce. The metal-to-oxygen-to-metal charge transfer should be favored in the low-temperature form, explaining the higher abundance of Fe^{3+} in the α form.

3.2. Influence of the Magnesium Concentration in (Fe,Mg)MoO_4 Samples. The second part of the results is devoted to the impact of the magnesium rate in $Fe_{1-x}Mg_xMoO_4$ mixed compounds on their structural parameters, the optical properties, and the piezochromic behavior. The XRD patterns corresponding to the as-prepared (Fe,Mg)-MoO_4 samples with different Fe/Mg ratios are collected in Figure 9. The diffraction maxima can be ascribed in all cases to the monoclinic β-phase, and the narrow diffraction peaks suggest a micrometric particle size for the prepared samples. The structural parameters of the β-phase have been determined by full pattern matching refinement of these diagrams, employing the space group $C2/m$. The values are collected in

DOI: 10.1021/ic5025845
Inorg. Chem. 2015, 54, 2176−2184

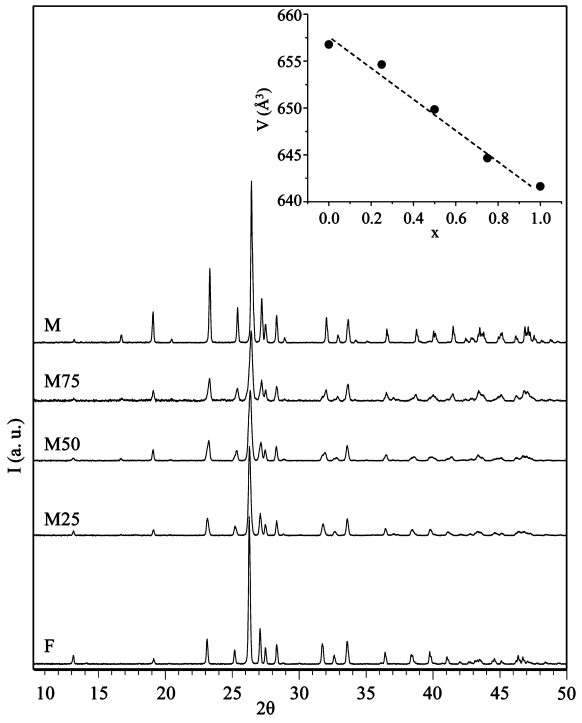

Figure 9. X-ray diffraction (XRD) patterns corresponding to the as-prepared (Fe,Mg)MoO_4 samples. The inset shows the evolution of the cell volume with the magnesium content.

Table 1, together with the reliability factors and the structural parameters of the α-phase for each sample. The cell parameters corresponding to the α-phase were determined by full pattern matching of the diagrams corresponding to the powder obtained after applying the highest pressure value in the piezochromic study. For this pressure value, the highest $\beta \rightarrow \alpha$ transformation with a resulting mixture of both crystallographic phases (discussed below) was found. To compare the piezochromic behavior of each sample, the α/β phase ratio was determined by Rietveld refinement of the corresponding X-ray diagrams. The percentages are indicated in Table 1. As can be observed in the table, there is a decrease in the cell parameter values for both phases with the increase of the magnesium content, because Mg^{2+} presents a lower ionic radii (0.72 Å) than Fe^{2+} (0.77 Å).[32] In this sense, the cell volume dependence with the magnesium content for the β-phase (see inset of Figure 9) and the linear fitting suggest a dependence that follows Vegard's law.

The $\beta \rightarrow \alpha$ phase transformation versus pressure curve is represented in Figure 10 for each (Fe,Mg)MoO_4 sample, considering the final α/β proportion previously determined by XRD. The P_{tr} value for each sample collected in Table 3 has been estimated for 50% transformation and, as represented in the upper side of Figure 8, it increases as the magnesium content increases. This effect has been related with the lower electronegativity of Mg^{2+}, which stabilizes the low-coordination form[9] that corresponds to the structure of the β-phase, for which the Mo atoms are located in tetrahedral sites, instead of presenting octahedral coordination as in the α-phase. In accordance with this β-phase stabilization effect, a higher content of the remnant β-phase for the last pressure value applied is observed.

The Kubelka–Munk transformation of the diffuse reflectance spectra versus photon energy corresponding to nonpressed (β-phase) (Fe,Mg)MoO_4 samples are represented in Figure 11a. By comparison of the different spectra, two phenomena are observed. First, a decrease in the d–d band intensity is observed with increasing magnesium content, which is related to a lower Fe^{2+} content, although a lower refractivity index due to a lower crystal density should also be considered. A CTB displacement to the UV region from the F sample to the M75 sample is also observed. This can be justified by taking into account the lower electronegativity of Mg^{2+}, in comparison with Fe^{2+}, which promotes more covalent Mo–O bonds.[9] The E_g values corresponding to the β-phase are collected in Table 3 for each (Fe,Mg)MoO_4 sample. The K/S transformation of the diffuse reflectance versus photon energy spectra of the samples subjected to the final pressure value (see phase transformation curve of Figure 11, discussed above) are depicted in Figure 11b. The observed phenomenology is a consequence of the mixture of β and α phases in the samples, and the estimated E_g values for this case have been collected in Table 3. The values are lower than those obtained for the nonpressed samples. The structure corresponding to the α-phase obtained after the pressure application is characterized by the presence of Mo atoms in octahedral sites. This higher coordination than in the case of the β-phase implies lower Mo–O bond covalence associated with a lower energy for the $O^{2-} \rightarrow Mo^{6+}$ CTB. This is the origin of the brown and black color for the nonpressed (β) and pressed (β+α) samples, respectively. By comparison of

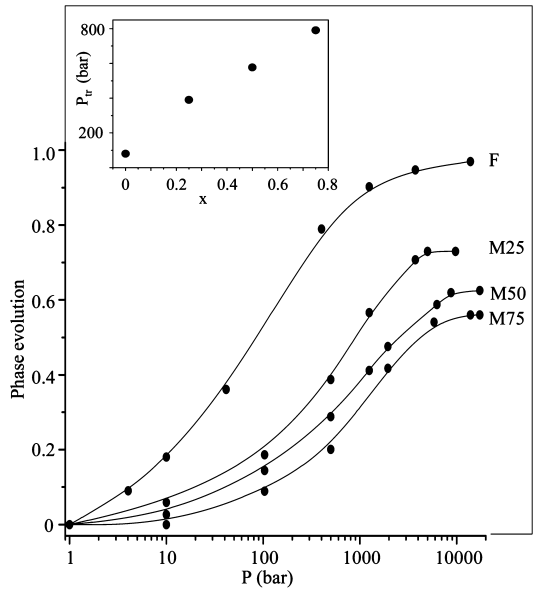

Figure 10. Phase transformation (P_{tr}) with pressure from the $\beta \rightarrow \alpha$ form for the different (Fe,Mg)MoO_4 samples. The evolution of the P_{tr} value with the magnesium content is represented along the upper side of the figure.

Table 3. $\beta \rightarrow \alpha$ Transition Pressure Values for the Different Samples; Band-Gap Values for the Samples before and after Pressure Are Also Shown

		E_g (eV)	
sample	P_{tr} (bar)	nonpressed, β	pressed, $\beta + \alpha$
F	80	1.70	1.1
M25	390	1.85	1.1
M50	577	1.95	1.15
M75	791	2.15	1.20

DOI: 10.1021/ic5025845
Inorg. Chem. 2015, 54, 2176–2184

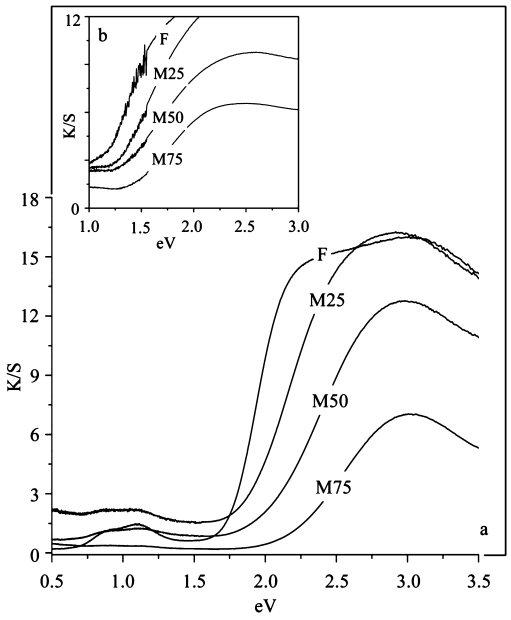

Figure 11. Kubelka–Munk transformation spectra (K/S) for the (Fe,Mg)MoO_4 samples (a) before pressure has been applied (β-phase), and (b, shown as an inset) after pressure has been applied (β and α phase).

the spectra corresponding to the pressed samples, the same effect of the lower electronegativity of the Mg^{2+} cations in the CTB position is observed.

Figure 12 shows the evolution of E_g with the content of magnesium for both situations, before pressing (β) and after

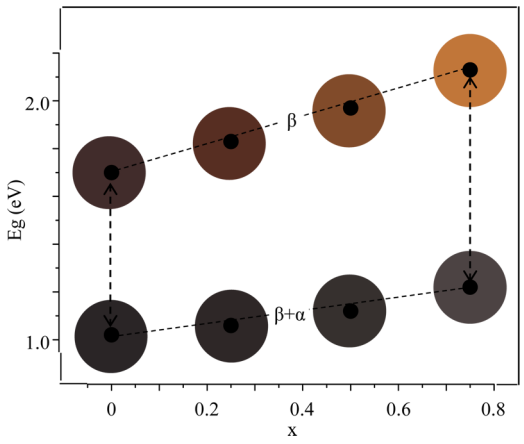

Figure 12. Evolution of E_g, relative to the magnesium content (x) before pressing (upper graph) and after pressing (lower graph). The evolution has also been illustrated by the experimental color that each sample showed before and after the application of pressure.

pressing (α+β). A slightly more abrupt slope is observed in the case of the graph corresponding to the β-phase (nonpressed samples, upper side). This implies a higher difference between the E_g values of the nonpressed and pressed forms for the M75 sample than for the F sample (indicated by arrows in the drawing). The color of the piezochromic samples before and after pressure application is also illustrated in the figure. The color shown is based on the experimental RGB coordinates. By visual analysis, one can assume a paler color with the increment of the magnesium content and also a higher optical contrast between the nonpressed and pressed forms of the M75 sample than in the case of the samples with lower magnesium content. This higher optical contrast between the nonpressed and pressed samples when increasing the magnesium content may be related to an increasing difference between the E_g values for the samples before and after the application of pressure.

4. CONCLUSION

In previous works, Sleight et al.[18] showed three modifications of $FeMoO_4$, based on XRD, Mössbauer, and magnetic susceptibility investigations. Two low-pressure forms, α and β, which crystallize with monoclinic unit cells (space group $C2/m$), have been considered in this paper. Based on the optical absorption and magnetic susceptibility measurements at low temperature, the $\beta \rightarrow \alpha$ transition of $FeMoO_4$ has been investigated for the first time. The $\beta \rightarrow \alpha$ pressure transition has been determined and reveals the good performance of the $FeMoO_4$ phase as a low-pressure sensor (80 bar transition pressure, uniaxially). Moreover, the Mössbauer spectra show the occurrence of two Fe^{2+} sites for the β phase with a small amount of Fe^{3+}cations, because of a charge transfer reaction involving Fe^{2+}/Fe^{3+} and Mo^{6+}/Mo^{5+} redox couples. Based on the site distortion and the structural features, the two quadripolar doublets of the β phase have been clearly affected. The four sites observed by Mössbauer spectroscopy for the α+β phases mixture can be classified in terms of site distortion. The Fe^{3+} content increases in the α+β phases mixture, in good agreement with the magnetic susceptibility. The occurrence of Mo^{6+} in the octahedral site in the α phase contributes to stabilizing more Mo^{5+} by O/Mo charge transfer and then more Fe^{3+} by O/Fe charge transfer. Finally, the Mg^{2+} substitution for Fe^{2+} ions allows the increase of the $\beta \rightarrow \alpha$ transition pressure (equivalent to decrease the $\alpha \rightarrow \beta$ transition temperature), because of the increase of the (Fe,Mg)–O bond iconicity, which contributes stabilizing the β phase with covalent Mo^{6+}–O bonds stabilized in Td sites (competitive bonds). The knowledge of the Fe^{2+} local environments and sites distortion, the occurrence of Fe^{3+} stabilized in $FeMoO_4$, and the variation of the optical absorption properties and band gaps for the α and β forms of $FeMoO_4$ lead to the design of new piezochromic pigments by tuning the Fe–O iono-covalent bond.

AUTHOR INFORMATION

Corresponding Author

*E-mail: gaudon@icmcb-bordeaux.cnrs.fr.

Notes

The authors declare no competing financial interest.

ACKNOWLEDGMENTS

The authors are thankful to L'Agence Nationale de la Recherche for financial support, under the ChoCoComp project (No. ANR-13-RMNP-0011).

REFERENCES

(1) Gaudon, M.; Deniard, P.; Demourgues, A.; Thiry, A.-E.; Carbonera, C.; Le Nestour, A.; Largeteau, A.; Létard, J. F.; Jobic, S. *Adv. Mater.* **2007**, *19*, 3517–3519.

(2) Blanco-Gutierrez, V.; Demourgues, A.; Gaudon, M. *Dalton Trans.* **2013**, *42*, 13622–13627.

(3) Rodriguez, F.; Hernandez, D.; Garcia-Jaca, J.; Ehrenberg, H.; Weitzel, H. *Phys. Rev. B: Condens. Matter* **2000**, *61*, 497–501.

(4) Gaudon, M.; Thiry, A. E.; Largeteau, A.; Deniard, P.; Jobic, S.; Majimel, J.; Demourgues, A. *Inorg. Chem.* **2008**, *47*, 2404–2410.

DOI: 10.1021/ic5025845
Inorg. Chem. 2015, 54, 2176–2184

(5) Gaudon, M.; Carbonera, C.; Thiry, A. E.; Demourgues, A.; Deniard, P.; Payen, C.; Létard, J. F.; Jobic, S. *Inorg. Chem.* **2007**, *46*, 10200−10207.
(6) Byrne, P. J.; Richardson, P. J.; Chang, J.; Kusmartseva, A. F.; Allan, D. R.; Jones, A. C.; Kamenev, K. V.; Tasker, P. A.; Parsons, S. *Chem.—Eur. J.* **2012**, *18*, 7738−7748.
(7) Takagi, H. D.; Noda, K.; Itoh, S. *Platinum Met. Rev.* **2004**, *48*, 117−124.
(8) Seeboth, A.; Loetzsch, D.; Ruhmann, R. *Am. J. Mater. Sci.* **2011**, *1*, 139−142.
(9) Righetti, L.; Robertson, L.; Largeteau, A.; Vignoles, G.; Demourgues, A.; Gaudon, M. *ACS Appl. Mater. Interfaces* **2011**, *3*, 1319−1324.
(10) Robertson, L. C.; Gaudon, M.; Jobic, S.; Deniard, P.; Demourgues, A. *Inorg. Chem.* **2011**, *50*, 2878−2884.
(11) Tian, S.; Zhang, J.; Chen, J.; Kong, L.; Lu, J.; Ding, F.; Xiong, Y. *Ind. Eng. Chem. Res.* **2013**, *52*, 13333−13341.
(12) Tian, S. H.; Tu, Y. T.; Chen, D. S.; Chen, X.; Xiong, Y. *Chem. Eng. J.* **2011**, *169*, 31−37.
(13) Jindal, R.; Gupta, H. C.; Sinha, M. M. *Philos. Mag.* **2014**, *94*, 208−220.
(14) Maione, A.; Devillers, M. *J. Solid State Chem.* **2004**, *177*, 2339−2349.
(15) Sowa, H. *Solid State Sci.* **2005**, *7*, 73−78.
(16) Kersen, U.; Holappa, L. *Appl. Phys. A: Mater. Sci. Process.* **2006**, *85*, 431−436.
(17) Ehrenberg, H.; Svoboda, I.; Wiesmann, M.; Weitzel, H. *Acta Crystallogr., Sect. C: Cryst. Struct. Commun.* **1999**, *C55*, 1383−1384.
(18) Sleight, A. W.; Chamberland, B. L.; Weiher, J. F. *Inorg. Chem.* **1968**, *7*, 1093−1098.
(19) Shahri, Z.; Salavati-Niasari, M.; Mir, N.; Kianpour, G. *J. Cryst. Growth* **2014**, *386*, 80−87.
(20) Zhang, L.; Cao, X. F.; Ma, Y. L.; Chen, X. T.; Xue, Z. L. *New J. Chem.* **2010**, *34*, 2027−2033.
(21) Ding, Y.; Wan, Y.; Min, Y. L.; Zhang, W.; Yu, S. H. *Inorg. Chem.* **2008**, *47*, 7813−7823.
(22) Eda, K.; Kato, Y.; Ohshiro, Y.; Sugitani, T.; Whittingham, M. S. *J. Solid State Chem.* **2010**, *183*, 1334−1339.
(23) Lagorio, M. G. *J. Chem. Educ.* **2004**, *81*, 1607−1611.
(24) Leeuwen, R.; Hung, C. J.; Kammler, D.; Switzer, J. A. *J. Phys. Chem.* **1995**, *99*, 15247−15252.
(25) Zhanga, Z.; Hua, C.; Hashima, M.; Chenb, P.; Xiong, Y.; Zhanga, C. *Mater. Sci. Eng., B* **2011**, *176*, 756−761.
(26) Marik, S.; Moran, E.; Labrugere, C.; Toulemonde, O.; Alario-Franco, M. A. *J. Solid State Chem.* **2012**, *191*, 40−45.
(27) Dey, S.; Ricciardo, R. A.; Cuthbert, H. L.; Woodward, P. M. *Inorg. Chem.* **2014**, *53*, 4394−4399.
(28) Thongkanluang, T.; Wutisatwongkul, J.; Chirakanphaisarn, N.; Pokaipisit, A. *Adv. Mater. Res.* **2013**, *770*, 3327−3330.
(29) Jose, S.; Prakash, A.; Laha, S.; Natarajan, S.; Reddy, M. L. *Dyes Pigm.* **2013**, *107*, 118−126.
(30) Sameera, S. F.; Rao, P. P.; Kumari, L. S.; James, V.; Divya, S. *Chem. Lett.* **2013**, *42*, 521−523.
(31) Ehrenberg, H.; Wltschek, G.; Trouw, F.; Kroener, T.; Weitzel, H.; Fuess, H. *J. Magn. Magn. Mater.* **1994**, *135*, 355−360.
(32) Shannon, R. D. *Acta Crystallogr., Sect. A: Cryst. Phys., Diffr., Theor. Gen. Crystallogr.* **1976**, *A32*, 751−767.

DOI: 10.1021/ic5025845
Inorg. Chem. 2015, 54, 2176−2184